Multifunctional Materials

PAPER • **OPEN ACCESS**

Soft actuators using liquid crystal elastomers with encapsulated liquid metal joule heaters

Multifunctional Materials

CrossMark

OPEN ACCESS

RECEIVED
15 January 2020

REVISED
24 March 2020

ACCEPTED FOR PUBLICATION
25 March 2020

PUBLISHED
1 June 2020

PAPER

Soft actuators using liquid crystal elastomers with encapsulated liquid metal joule heaters

Teresa A Kent[1,2], Michael J Ford[1], Eric J Markvicka[2,3] and Carmel Majidi[1,2,4]

[1] Mechanical Engineering, Carnegie Mellon University; Pittsburgh, Pennsylvania 15213, United States of America
[2] Robotics Institute, Carnegie Mellon University; Pittsburgh, Pennsylvania 15213, United States of America
[3] Mechanical & Materials Engineering, University of Nebraska-Lincoln; Lincoln, Nebraska 68588, United States of America
[4] Author to whom any correspondence should be addressed.

E-mail: cmajidi@andrew.cmu.edu

Keywords: liquid crystal elastomers, electromigration, liquid metal, soft actuator, shape memory, joule heater

Supplementary material for this article is available online

Abstract

We present a soft actuator composed of fluidic channels of liquid metal alloy embedded in a liquid crystal elastomer (LCE). The LM channels function as stretchable Joule heating elements that deliver heat to the LCE to induce a shape memory phase transition. Because the heater is fluidic, it can deform with the surrounding LCE as the actuator extends and contracts during actuation. In addition to contractile actuation, the LCE can be programmed to perform in-plane or out-of-plane flexural actuation, which exhibit deformations predictable using a simple finite element analysis model. By combining a liquid metal heater with a shape memory polymer, we achieve a soft actuator that does not require an external heat source and can instead be directly activated with electrical current. Finally, we show that the liquid metal channels can also function as a sensor during the actuation cycle, allowing for closed-loop control of the soft actuator.

1. Introduction

Soft machines can exhibit functions that are difficult to achieve with rigid hardware. For example, limbed robots made with soft materials can squeeze through confined spaces [1, 2] and continue to operate after being crushed [3] or punctured [4]. Moreover, soft machines and robots can easily adapt to uneven terrains [5] and grasp complex shapes [6, 7]. However, despite tremendous advancements in the development of these systems, further progress depends on continued development of 'artificial muscle' actuators that can reversibly change shape and perform mechanical work in response to controlled stimulation. Of particular interest are shape memory materials that have the intrinsic ability to change shape when stimulated with heat, light, electric field, or electricity. While existing shape-morphing materials are promising, there is room for improvement in addressing trade-offs related to form factor, shape-memory responsiveness, compliance, deformability, actuation speed, actuation work output, and compatibility with miniaturizable and mobile supporting hardware [8, 9].

Examples of shape-morphing materials that have been used in soft robotics include nickel titanium alloy [10] (e.g. Nitinol), shape memory polymers [11], and liquid crystal elastomers (LCEs). LCEs are especially attractive because they exhibit large linear shape change (up to 400%) [12, 13] and are printable [14–17]. LCEs can also be programmed with specified orientations of liquid crystal monomers to create complex modes of reversible deformation (e.g. Gaussian curvature) [18–22]. Despite their promise, LCEs typically require external heating elements or stimuli-responsive inclusions/chemical modifications to facilitate the liquid crystal phase transition and subsequent shape change, which has significantly inhibited their applications in soft robotics [23].

Previously, researchers have engineered LCE composites capable of electrically-activated actuation using silver ink [24], flexible wires [25–30], graphite circuits [31, 32] and carbon coatings [33, 34] for Joule heating. While rigid fillers/heating elements have proven successful for repeatable actuation, they introduced mechanical constraints to the actuators and limited complex actuation modes (e.g. flexural deformation)

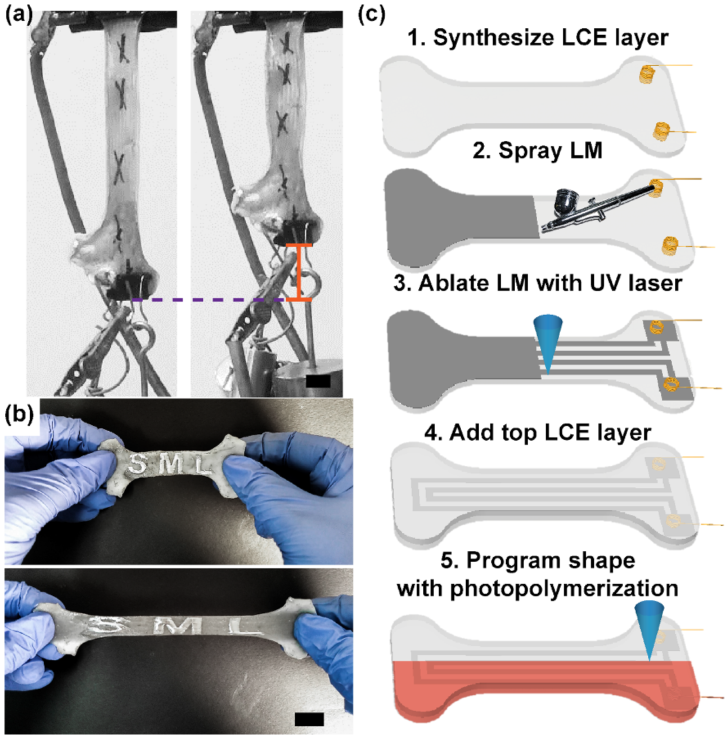

Figure 1. (a) Actuation by Joule heating is accomplished using an embedded liquid metal (LM) heater between two liquid crystal elastomer (LCE) layers, connected to an external power supply by copper coils. LM Joule heaters can heat the soft actuator above the transition temperature (e.g. >75 °C)(figure S.9a in the Supplementary Information (stacks.iop.org/MFM/3/025003/mmedia))) and enable lifting of payloads >40 times the weight of the soft actuator. Scale bar represents 10 mm. (b) As the LCE stretches, the LM stretches with the LCE, staying conductive without impeding the strain. Scale bar represents 20 mm. (c) Step-by-step schematic describing fabrication of UV laser-ablated Liquid Metal (LM) Joule heaters atop LCEs. See section S.VI-B2 in the SI for details.

[24, 25]. One promising approach used multiple patterned heaters to create complex actuation but could not achieve full linear actuation while maintaining conductivity [28]. Another recent method utilizes serpentine traces of copper wiring embedded within a tubular LCE to control local heating and phase change [30].

Recently, our group synthesized a liquid metal-LCE composite capable of unencumbered Joule-heated actuation, but the composite was not capable of closed-loop control and contained a high content of liquid metal [35]. Here we introduce an improved method for creating fully soft LCE actuators that can be electrically actuated with an embedded LM heater (figure 1(a)). The soft artificial muscle developed here is distinct from previous efforts with LCE and embedded liquid metal. In this work, LM is spray coated to create a thin film that functions as an electrical heating element and has significantly less volume of liquid metal than the 50 vol. % percolating networks that had been reported for LCE-LM composites [35]. These patterned films of liquid metal are fully encapsulated and remain intact and electrically conductive when the surrounding elastomer is stretched (figure 1(b)) [36–43]. LM deformation causes a change in resistance permitting 'self-sensing' during actuation, where the LM channel is capable of simultaneously providing Joule heating while also detecting the actuator's deformation during the actuation cycle. Our fabrication process is simple and amenable to arbitrary geometries (figure 1(c)).

To achieve electrically-powered actuation with a LM-based Joule heater, we had to address the challenge of electromigration. Electromigration is a known concern in solid state circuits [44] and can cause open or short circuits [45]. Recent efforts have focused on the role of electromigration in limiting the amount of electrical current that can be transported through a thin trace of liquid metal [46, 47]. Here, we avoid electromigration failure through careful characterization and circuit design. As a result, electrically-powered actuation through thermal stimulation can be controlled and localized by Joule-heating (figure 1(a)). Using this approach, we achieve a work density of 9.2 J kg^{-1} and maximum contractile strain of 50 %.

2. Materials and methods

2.1. Electromigration

The figure of merit for electromigration is the mean time to failure (MTF) as described by Black's equation: $MTF = A/j^m \times e^{Q/kT}$. Here A is the cross-sectional area of the current carrying element; j is the applied current; m is a model parameter; Q is the activation energy; k is Boltzmann's constant; and T is the temperature [44]. The model parameter for liquid gallium thin films was measured to be $m = 3.2$ [46]. This relatively high value suggests that LM is highly susceptible to circuit failure, especially at the high current used in Joule heating.

We characterized the influence of electromigration by subjecting LM circuit traces to varying amounts of electrical power. LM traces were spray deposited atop polydimethylsiloxane (PDMS, Sylgard 184) using a Master Airbrush and laser-cut stencil that was patterned from Blazer Orange Laser Mask Tape using a CO_2 laser (VLS 3.50; Universal Laser Systems). Eutectic gallium-indium (EGaIn, In and Ga from RotoMetals) was used as the LM alloy due to its low viscosity (1.99×10^{-3} Pa s), high conductivity (3.4×10^6 S m^{-1}), and negligible toxicity [40]. First, the maximum current that could be applied before failure was monitored. Current was applied to samples of four different widths and two different thicknesses on a substrate made with PDMS either uncovered or covered by a second layer of PDMS. The positive and negative terminals of the LM traces were $\geq$2.5 times the width of the channel [47] so that breakup could be observed in the narrow channels by optical microscopy rather than at the contacts [46]. Referring to figure 2(a), the contact area had a width of 5 mm, and the channel widths ranged from 0.5 mm to 2 mm, with a channel length of 5 mm. A KORAD KA3005P power supply supplied current using a ramp function that increased the current by 0.2 A every 30 seconds until breakup occurred, defined as the moment the power supply read an open circuit ($R \geq 10$ kΩ).

Next, we monitored the change in resistance as current was increased at set time intervals. For these measurements, LM channels (140 μm $\times$ 1 mm $\times$ 5 mm) were encapsulated in PDMS, and current was applied and increased at set time intervals of 30 s, 60 s, 90 s and 300 s until failure occurred. An 'unstable region' was defined as the point at which we observed a >15% increase of resistance. The effect of the current ramp and inverting polarity on electromigration failure was also evaluated. We applied five different current patterns after reaching the unstable region to determine how increasing current/changing the voltage polarity affected the resistance/breakup in the LM channel. The five current patterns involved increasing the current by 0.25 A every 90 s until reaching the unstable region, followed by immediately: (1) reducing the current to 0 A and restarting the ramp; (2) reducing the current by 0.5 A and holding for 10 minutes; (3) inverting the polarity and then restarting the ramp at the original polarity; (4) reducing the current to 0 A and ramping the current with the polarity inverted from the original ramp; and (5) inverting the polarity, reducing the current to 0 A, and ramping the current with the polarity inverted from the original ramp. For a visualization of the applied current pattern see figure S.8e-i in the SI.

2.2. LCE actuator fabrication and characterization

The entire process for the fabrication of the LCE actuator with LM channels is outlined in figure 1(c) and detailed in section S.VI(a-c) in the SI. LCEs were synthesized by adopting previously reported procedures [24, 48]. LM heaters were either patterned via UV laser ablation [49] with a LPKF Protolaser U3 or spray coated using a stencil mask (see section S.VI-B3 in the SI) [50–52]. Details on resolution and laser parameters are outlined in section S.VI-A in the SI. The first layer of LCE was fully cured with coiled copper wires embedded near the end of the LCE to make connection with the LM heaters. The LCE layer was then coated with a thin film of LM by spray deposition with an airbrush, with the coating either covering the entire sample for UV laser ablation or through a stencil mask. After the heater was sprayed/patterned, a second layer of LCE was used to encapsulate the heater to minimize heat loss to the environment, an improvement compared to external heaters used in previous reported methodologies [24, 25, 33].

Heaters were designed by considering an analytical model (section S.VI-C in the SI) that optimized the actuation speed. The model was based on (i) the number of heaters of specified dimensions and orientation that could fit in a prescribed bounding box, (ii) the maximum stable current as determined from electromigration tests, and (iii) the power required to heat the LCE significantly above the liquid crystal transition temperature (e.g., 80 °C when the transition temperature was 70 °C). Multiple parallel LM channels were preferred over a single tortuous LM channel since the parallel channels would divert current to the path of lowest resistance, thereby reducing the chance of failure by electromigration. Five heater designs were optimized (table S.I in the SI). Designs for the LCE-LM actuators were evaluated in an ANSYS model capable of activating the heater and determining the transient local contraction of the LCE (figure 3(d)). The model described in detail in section S.VI-D in the SI uses empirical normalized length change as a function of temperature [24] to determine temperature dependent coefficients of thermal expansion (CTEs).

As part of the LCE synthesis, an optional UV-activated cross-linking agent can be added to the uncured LCE mixture prior to base-catalyzed curing [48]. The liquid crystal orientation can be selectively programmed when the LCE is exposed to UV light, making the LCE capable of zero-stress actuation from one shape to another. We selectively programmed different sections of the LCE (figure 3) using a LPKF UV Laser, which has increased precision relative to a shadow mask. The optimum laser parameters to initiate photopolymerization were found to be one repetition at a laser power of 0.4W with a mark speed of

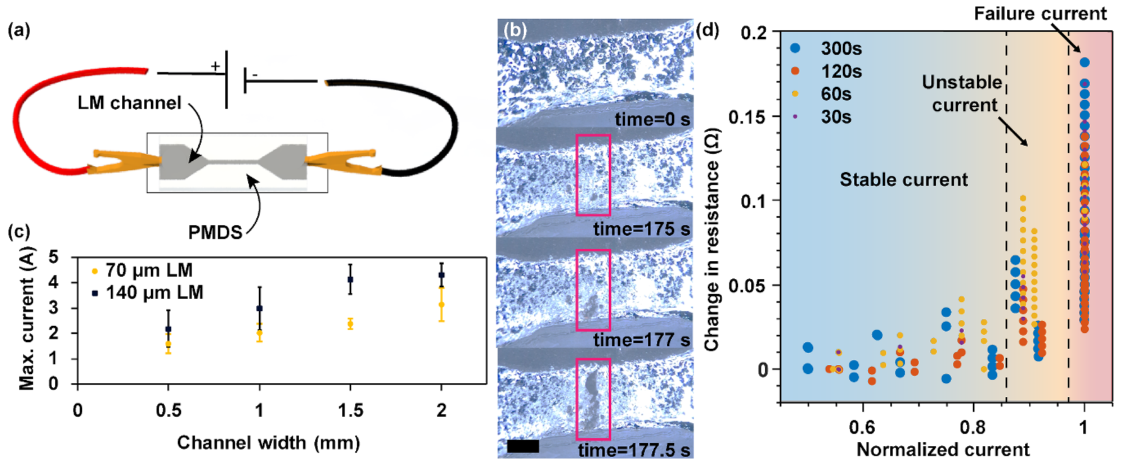

Figure 2. a) Schematic of electromigration test set up illustrating the power supply connection to the LM circuit. b) Optical micrographs of a 2 mm × 5 mm × 140 μm liquid metal (LM) channel as a current ramp is applied until electromigration occurs. The scale bar represents 1 mm c) Maximum current where electromigration leads to an open circuit as a function of LM channel width (n = 5 samples). Yellow and black data points correspond to LM film thicknesses of 70 μm and 140 μm, respectively. Error bars represent standard deviation. d) Change in resistance vs. normalized current for a 140 μm x 1 mm × 5 mm channel, where normalized current is calculated as the measured current divided by the current at failure.

200 mm s^{-1} and a 250 μm *z*-axis focal offset using the XY hatch pattern. Full laser settings can be found in figure S.2 in the SI. After initial photopolymerization by the UV laser, we heated the LCE above the isotropic temperature and allowed it to cool, and then exposed the entire LCE with a UVL-56 Handheld UV Lamp (6 Watt, 365nm) for five minutes to ensure the UV crosslinker was completely reacted. Complex shape-morphing of UV laser-programmed LCEs could be modeled in ANSYS to approximate the shape change caused by different localized programmed strains.

LCE actuators with LM channels were powered using a programmable power supply (KA3005P or KA3010P, KORAD). For actuation characterization, the LM heaters were subjected to a ramped current increasing 0.25 A every 90 s starting from 1 A below the expected unstable region associated with electromigration. Current was applied until the resistance increased by 15% at which point the current was reversed for five seconds. Actuation testing was then completed at 0.5 A below the threshold 'unstable current' unless otherwise stated. Contractile and bending actuation were tracked using a digital camera and tracking code in Python. Actuation work densities for contractile actuation of multiple samples and heater designs were determined by tracking the position of the actuator as it lifted successively higher weights until mechanical failure occurred. For the actuation work density tests, electrical current was applied for five minutes followed by a cooling time of five minutes. Contractile actuation speed was evaluated for two heater designs by increasing the power and measuring the time for a strained LCE to return to its original length. For closed-loop control of the soft actuator, the current and voltage applied to the LM channel was measured by the programmable power supply and recorded using a script in MATLAB. According to Ohm's law, the resistance of the LM channel is expected to change as the actuator is heated and contracts. Actuators were initially screened to develop a heuristically-determined threshold in the change in resistance as a function of time, which was used to control when actuation would start and end.

3. Results and Discussion

3.1. Electromigration characterization

Before LCEs with LM Joule heaters could be fabricated, we needed to first evaluate electromigration in the LM channels. When a LM channel was subjected to an increasing current until it failed, the maximum temperature it reached was 34 °C before failing by electromigration (figure S.8b,c in the SI), which would not be adequate for activating the LCE. To observe electromigration, LM channels with large contact areas were subjected to electrical power until breakup progressed to an open circuit (figure 2(a)). For example, when current was applied to the LM channel for 177 s, breakup of the channel was observed by optical microscopy (figure 2(b)). In particular, we found that the channel was intact and conductive at 0 s and 175 s. Once signs of deterioration are visible (*e.g.*, at 177 s) the electrical conductivity is lost ($R \geq 10$ kΩ) in less than 1.5 s (*e.g.*, at 177.5 s).

We then measured the maximum current that could be applied before electromigration occurs, causing an open circuit. We observed that the maximum current increased with increasing channel width and channel thickness (figure S.8j in the SI). By encapsulating the LM channel with another elastomer layer, the maximum current could be further increased (figure 2(c)). Temperature and time are also important factors in electromigratory breakup [44]. However under our testing conditions, we experimentally determined that temperature and time had negligible impact relative to current density (section S.VI-E in the SI), consistent with a high model parameter, *m*, in Black's equation.

By monitoring current as a function of time, we observed electrical indications preceding electromigration break up (figure 2(d)); i.e. as electromigration occurs, the resistance increases. Referring to figure 2(d), each step of supplied current was applied to the channel for 30 s (purple), 60 s (yellow), 120 s (orange), and 300 s (blue). The plot is subdivided into three regions: where current and resistance are stable; where current and resistance become unstable; and where the channels fail. When the current density is low, the resistance in the channel remains constant. However, when the conductive channel is within 0.5 A of failure, the resistance begins to increase by >15% of the original value. At this point, an open circuit will occur within 90 s, Therefore, by monitoring the resistance while applying current that is close to the failure current, we could identify and characterize regions of stable current, unstable current, and failure (figure 2(d)). By utilizing the change in resistance as an indicator for failure we can avoid failure and enable effective Joule heating.

Using the change in resistance as a marker for electromigration, we studied the effect of applying five distinct current ramps to LM channels (section S.VIE2 in the SI). As a baseline, current in a LM channel was increased by 0.25 A every 90 s until the current reached the unstable region, at which point the current was immediately reduced to 0 A and the ramp was restarted. During the baseline test, electromigratory failure occurred within three repeated cycles (figure S.8e in the SI). In contrast, failure did not occur when the current in an identical LM channel was increased by 0.25 A every 90 s until the current reached the unstable region, followed by immediately reducing the current by 0.5 A and holding for 10 minutes (figure S.8f in the SI). When the current in identical LM channels were subjected to three different current ramps that all involved inverting the voltage polarity, each LM channel survived through eight repeated cycles and only failed after holding the current in the unstable region after cycling (figure S.8g-i in the SI). To test the feasibility of Joule heating with LM channels, we applied a current value just below the unstable region and repeatedly switched the polarity on a LM channel, and the temperature reached 122 °C without electromigration failure occurring (figure S.8d in the SI), consistent with previous reports on electromigration in LM thin films where alternating current increased mean time to failure relative to direct current [46].

Electromigration was considered when designing LM heaters for the LCEs. Parallel heaters are the most suitable design since they can prevent an open circuit from rapidly propagating due to electromigration. For a heater composed of a single LM channel, void propagation occurred rapidly (figures 2(b) and (d)) when the current reached the unstable region. Void propagation is abrupt because once a void is formed, the current density increases as the cross sectional area decreases. This current density will continue to increase until the single LM channel fails. For parallel heaters, if a single parallel trace begins to fail, the remaining traces can still function, thus stabilizing the circuit as long as the total current can be reduced and remains outside the unstable region of the current.

3.2. LCE actuator fabrication and characterization

One of the biggest advantages of LM heaters relative to previously reported methods for heating LCE [24, 25, 28] is the compliant nature of the LM channels (figure 1(b)). This compliance is demonstrated by the LCE's ability to achieve a large actuation stroke (figure 1(a)). LCEs with LM heaters were capable of actuation strokes > 50 % and heating above the transition temperature (figure S.9(a), (c) in the SI).

Photopolymerization of the LCE permits actuation modes other than contractile actuation such as in-plane and out-of-plane bending. Photopolymerization with the LPKF laser increases precision for patterning and eliminates the need to create masks, making it an effective tool for rapid and cost effective prototyping of new photopolymerization patterns. Complex modes of actuation like in-plane and out-of-plane bending could be modeled by finite elemental analysis. From empirical results, we used a gradient of thermal expansion coefficients to predict transient behavior of LCEs during Joule heating. In-plane bending was programmed by photopolymerizing one side of the front/back of the sample in a contracted state while the other side of the front/back was photopolymerized in a stretched state. Finite element analysis in ANSYS predicted straightening and bending when above and below the transition temperature, respectively (figure 3(a)). Selective photopolymerization resulted in a 'multi-strain' design composed of alternating regions of the LCE in either a contracted or stretched state. We believe that this design might be useful in applications that require restriction of localized actuation; for example, placing rigid electronic components for sensing and signal processing atop regions where actuation is restricted. Again, the ANSYS model was consistent with the observed deformation (figure 3(b)).

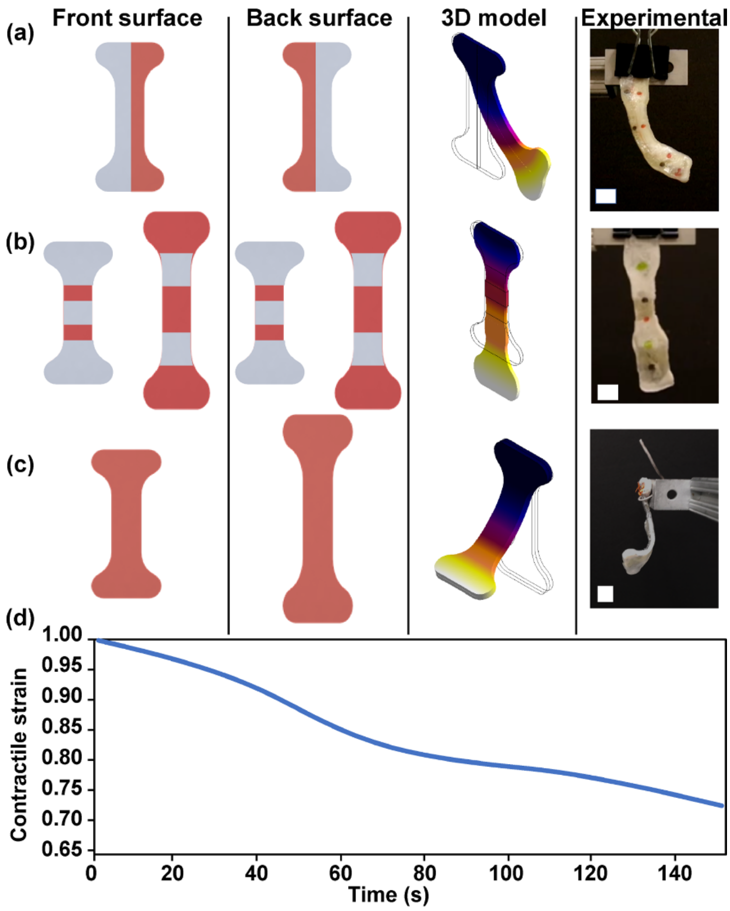

Figure 3. Using the UV laser patterning, liquid crystal elastomers (LCEs) were programmed to exhibit bending and flexing modes of actuation by exposing the front (column 1) and back (column 2) of the LCEs, as illustrated in the schematics. The expected shape change from the ANSYS model (section S.VI-D2 in the Supplementary Information) (column 3) and the experimental results (column 4) agreed for the (a) in-plane bend, (b) multi-strain, and (c) out-of-plane bend. Scale bars represent 10 mm. (d) Using an ANSYS model of the soft actuator, the contractile strain as a function of time was predicted for Joule-heating with LM. The model uses experimental data [24] to predict temperature-dependent shape-morphing (S.VI-D1 in the SI).

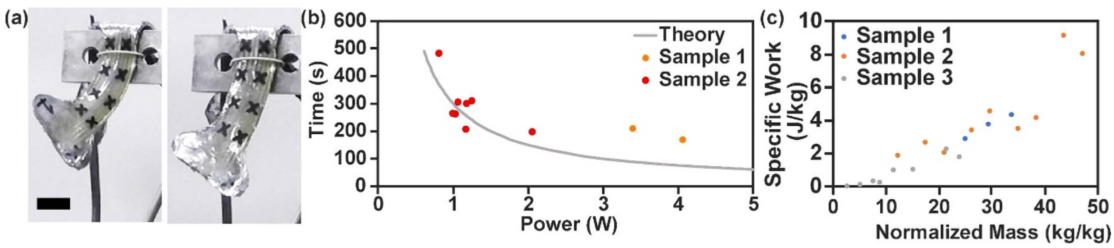

Figure 4. (a) Cycling of a liquid crystal elastomer (LCE) programmed to actuate with an in-plane bend. The LCE was successively heated by Joule-heating multiple times to $T > 60$ °C (figure S.9(c) in the Supplementary Information). Photographs show the LCE bending through Joule-heating. (b) Actuation time of the LCE as a function of the input power applied to the Joule heater tested with two distinct heater designs. The actuation time is the time required for the LCE to return to its contracted length with a hanging weight. The gray trace is the theoretical prediction for heating the LCE from 20°C to 80 °C as a function of power, based on the method discussed in section S.VI-C of the Supplementary Information. (c) Specific work vs. normalized mass for three LCE samples, where the specific work is the amount of work divided by the mass of the sample and the normalized mass is the mass of the load normalized to the mass of the sample.

The out-of-plane bending highlights an advantage of UV laser photopolymerization relative to photopolymerization with a shadow mask or surface templating since careful tuning of the laser parameters can direct the penetration depth so that the entire sample is not inadvertently cross-linked during each programming step. The front surface of the sample was patterned in the contracted state, followed by patterning of the back surface in the stretched state, which resulted in the out-of-plane bending predicted from the model and observed experimentally (figure 3(c)). Our simple computational model allows us to predict and validate complex shape-morphing for different patterns programmed into the LCE as well as the

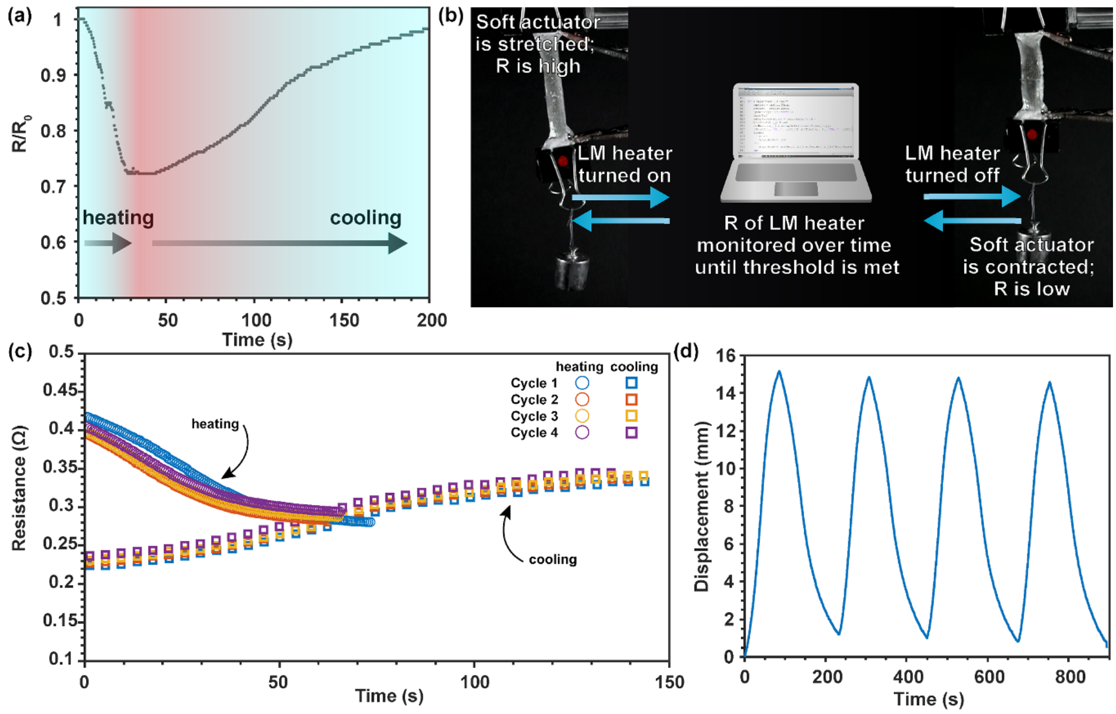

Figure 5. Closed-loop control of the soft actuator. (a) Normalized resistance as a function of time while heating the ambient environment with a heat gun, where the normalized resistance is the measured resistance (R) divided by the initial resistance (R_0). (b)Outline of closed-loop control where the resistance (R) of the soft actuator is high when the actuator is stretched. The power supply inputs power into the LM heater while simultaneously measuring resistance and is controlled by MATLAB. The user sets a threshold for the change in resistance as a function of time, and when the threshold is reached, the LM heater turns off. The soft actuator has contracted due to Joule-heated actuation, and the resistance is low. (c) Resistance as a function of time during heating and cooling when using closed-loop control. Threshold slopes of -0.0001 and 0.0001 Ω s^{-1} were used to turn off and on heating. During heating, the resistance decreased. During cooling, the resistance increased. (d) Actuator displacement as a function of time during actuation using closed-loop control.

transient effect of different Joule heater shapes (figure 3(d), figure S.7 in the SI). Such a model can aid in the deterministic design and operation of flexural LCE actuators with embedded Joule heating elements (figure 4(a)). As shown in figure 4(b), the agreement between theory and experiment is reasonable considering the simplicity of the computational model. Nonetheless, there are discrepancies since the simulation could be improved by accounting for the additional power required to heat up the embedded liquid metal, including the enthalpy for the phase transition of the liquid crystal phase, and improving accuracy of the specific heat of the LCE (see section.S.VI-C).

Importantly, LCE actuators with LM heaters achieved a work output that is similar to previously reported LCEs with similar mechanical properties [53]. Using Joule heating, the LCE is able to achieve a specific work density up to 9.2 J kg^{-1} (figure 4(c)), comparable to mammalian muscle [54]. As the load increased, the specific work density of the LCE increased not only because of the increased load but also because the increased load produces higher actuation strains. LCEs are reported with a range of specific work density on the order of 1-1000 J kg^{-1} with the specific value typically depending on LCE chemistry, processing, and method of actuation [12, 21, 35, 55]. These tests also demonstrated the durability of the actuator and heater architecture because the same samples were actuated for $\geq$8 weights per sample before failing mechanically rather than electrically.

We previously synthesized a LM-LCE composite capable of Joule-heated actuation [35]. One notable difference of these embedded LM Joule heaters relative to our previous report is the electromechanical coupling, where changes in resistance of the LM Joule heater can be correlated to changes in strain, which was not possible for the composite. By slowly heating the ambient environment while measuring the resistance, changes in resistance were observed during ambient heating and cooling (figure 5(a)). Changes in resistance through actuation strain were also measured with Joule-heating (figure S.9(b) in the SI). In the stretched state, the soft actuator had higher resistance than in the contracted state. Using the change in resistance, we achieved closed-loop control of the soft actuator, where the LM Joule heater has an additional function of sensing (figure 5(b)). The soft actuator is thus 'self-sensing', meaning that the material architecture processes and responds to its environment without dependency on rigid, on-board sensing elements/chips [56]. For closed-loop control, the power supply delivered power to the LM heater and simultaneously measured the resistance as a function of time, using a script in MATLAB to record and process data. The resistance changed during heating because of changes in temperature and electromechanical coupling. Once the change in resistance as a function of time reached a threshold as defined by the user, the power supply turned off to allow the soft actuator to cool and return to its stretched state. While cooling, a small pulse of voltage (e.g. 0.03 V) was periodically applied to probe the resistance until a new threshold was reached. Note that at low voltages like 0.03 V, the KORAD power supply consistently measured lower resistance values than at higher voltages but was still reliable enough to measure changes in strain and control actuation. While heating (or cooling), the resistance could consistently decrease (or increase) until reaching the specified threshold (figure 5(c)). In this way, repeatable Joule-heated actuation was possible with closed-loop control (figure 5(d)).

4. Conclusion

Here, we demonstrated electrically-activated LCEs that use embedded LM Joule heaters capable of programmable shape change and intrinsic sensor feedback. A key benefit of LM traces relative to previous iterations of embedded and external Joule-heaters is that the LM traces are compliant and deformable. Notably, the soft artificial muscle reported here was able to use the LM as both a heating element and a sensor for tracking its own position, which was not possible for previous embodiments [35]. A significant challenge we were able to overcome in using LM heaters is the phenomenon of electromigration. Specifically, we show that the heaters can be calibrated and designed to overcome limitations introduced by electromigration in order to achieve successful actuation of LCEs. A finite elemental analysis model of the LCEs, where the LCEs were treated as materials with a gradient of thermal expansion coefficients, proved an effective predictive tool for determining transient behavior of LCEs during Joule heating. Gradient coefficients of thermal expansion across an LCE were similarly shown to effectively predict complex shape-morphing capabilities of photoinititated LCEs. From this work, LM-embedded LCEs can be modified and designed to meet criteria for actuation in robotics and shape programmable materials.

4. Acknowledgment

The authors would like to thank Keene Chin for developing the code used to track the LCE actuation. This research was supported by Air Force Office of Scientific Research (AFOSR) Multidisciplinary University Research Initiative (FA9550-18-1-0566; Program Manager: K Goretta).

ORCID iDs

Teresa A Kent https://orcid.org/0000-0002-6935-9586
Michael J Ford https://orcid.org/0000-0001-7118-2479
Eric J Markvicka https://orcid.org/0000-0002-5463-1567
Carmel Majidi https://orcid.org/0000-0002-6469-9645

References

[1] Huang X, Kumar K, Jawed M K, Nasab A M, Ye Z, Shan W and Majidi C 2018 Chasing biomimetic locomotion speeds: Creating untethered soft robots with shape memory alloy actuators *Science Robot.* **3** eaau7557
[2] Shepherd R, Ilievski F, Choi W, Morin S, Stokes A, Mazzeo A, Chen X, Wang M and Whitesides G 2011 Multigait soft robot *Proc. Natl Acad. Sci. USA* **108** 20400–3
[3] Tolley M T Shepherd B, Mosadegh K C Galloway M, Karpelson M, Wood R J and Whitesides G M 2014 A resilient, untethered soft robot *Soft Robot.* **1** 213–23
[4] Markvicka E J and Huang X and Majidi C 2018 An autonomously electrically self-healing liquid metal–elastomer composite for robust soft-matter robotics and electronics *Nat. Mater.* **17** 618
[5] Huang X, Kumar K, Jawed M, Ye Z and Majidi C 2019 Soft electrically actuated quadruped (seaq)-integrating a flex circuit board and elastomeric limbs for versatile mobility *IEEE Robot. Automat. Lett.* https://doi.org/10.1109/LRA.2019.2903856
[6] Brown E, Rodenberg N, Amend J, Mozeika A, Steltz E, Zakin M R, Lipson H and Jaeger H M 2010 Universal robotic gripper based on the jamming of granular material *Proc. Natl Acad. Sci.* vol 107 pp 18809–14
[7] Cianchetti M, Calisti M, Margheri L, Kuba M and Laschi C 2015 Bioinspired locomotion and grasping in water: the soft eight-arm octopus robot *Bioinsp. Biomimet.* **10** 035003
[8] Kim S, Laschi C and Trimmer B 2013 Soft robotics: a bioinspired evolution in robotics *Trends Biotechnol.* **31** 287–94
[9] Rich S I, Wood R J and Majidi C 2018 Untethered soft robotics *Nat. Electron.* **1** 102
[10] Seok S, Onal C D, Cho K-J, Wood R J, Rus D and Kim S 2012 Meshworm: a peristaltic soft robot with antagonistic nickel titanium coil actuators *IEEE/ASME Trans. Mechatron.* **18** 1485–97
[11] Takashima K, Rossiter J and Mukai T 2010 Mckibben artificial muscle using shape-memory polymer *Sensors Actuators* A **164** 116–24

[12] Saed M O, Torbati A H, Nair D P and Yakacki C M 2016 Synthesis of programmable main-chain liquid-crystalline elastomers using a two-stage thiol-acrylate reaction *JoVE J. Visual. Exp.* **107** e53546
[13] Wermter H and Finkelmann H 2001 Liquid crystalline elastomers as artificial muscles *e-Polymers* **1**
[14] Ambulo C P, Burroughs J J, Boothby J M, Kim H, Shankar M R and Ware T H 2017 Four-dimensional printing of liquid crystal elastomers *ACS Appl. Mater. Inter.* **9** 37332–9
[15] Kotikian A, Truby R L, Boley J W, White T J and Lewis J A 2018 3d printing of liquid crystal elastomeric actuators with spatially programed nematic order *Adv. Mater.* **30** 1706164
[16] López-Valdeolivas M, Liu D, Broer D J and Sánchez-Somolinos C 2018 4d printed actuators with soft-robotic functions *Macromol. Rapid Commun.* **39** 1700710
[17] Zhang C, Lu X, Fei G, Wang Z, Xia H and Zhao Y 2019 4d printing of liquid crystal elastomer with a controllable orientation gradient *ACS Appl. Mater. Inter.* https://doi.org/10.1021/acsami.9b18037
[18] Schuhladen S, Preller F, Rix R, Petsch S, Zentel R and Zappe H 2014 Iris-like tunable aperture employing liquid-crystal elastomers *Adv. Mater.* **26** 7247–51
[19] Fuchi K, Ware T H, Buskohl P R, Reich G W, Vaia R A, White T J and Joo J J 2015 Topology optimization for the design of folding liquid crystal elastomer actuators *Soft Matter* **11** 7288–95 vol
[20] McConney M E, V P Tondiglia K M Lee D, Smalyukh I I and White T J 2013 Topography from topology: photoinduced surface features generated in liquid crystal polymer networks *Adv. Mater.* **25** 5880–5
[21] Ware T H, McConney M E, Wie J J, Tondiglia V P and White T J 2015 Voxelated liquid crystal elastomers *Science* **347** 982–4
[22] Aharoni H, Xia, Y Zhang X, Kamien R D, and Yang S 2017 Making faces: Universal inverse design of surfaces with thin nematic elastomer sheets arXiv preprint arXiv:1710.08485, https://doi.org/10.1073/pnas.1804702115
[23] Cresta V, Romano G, Kolpak A, Zalar B and Domenici V 2018 Nanostructured composites based on liquid-crystalline elastomers *Polymers* **10** 773
[24] Yuan C, Roach D J, Dunn C K, Mu Q, Kuang X, Yakacki C M, Wang T, Yu K and Qi H J 2017 3d printed reversible shape changing soft actuators assisted by liquid crystal elastomers *Soft Matter* **13** 5558–68
[25] Minori A, Jadhav S, He Q, Cai S and Tolley M 2017 Reversible actuation of origami inspired composites using liquid crystal elastomers *ASME 2017th Conf. on Smart Materials, Adaptive Structures and Intelligent Systems, Pp.V001T08A015–V001T08A015* American Society of Mechanical Engineers https://doi.org/10.1115/SMASIS2017-3986
[26] Belmonte A, Lama G C, Cerruti P, Ambrogi V, Fernández-Francos X and De la Flor S 2018 Motion control in free-standing shape-memory actuators *Smart Mater. Struct.* **27** 075013
[27] Petsch S, Rix R, Reith P, Khatri B, Schuhladen S, Ruh D, Zentel R and Zappe H 2014 A thermotropic liquid crystal elastomer micro-actuator with integrated deformable micro-heater *2014 IEEE 27th Int. Conf. on Micro Electro Mechanical Systems (MEMS)* pp 905–8
[28] Wang C *et al* 2018 Soft ultrathin electronics innervated adaptive fully soft robots *Adv. Mater.* **30** 1706695 vol
[29] Frick C P, Merkel D R, Laursen C M, Brinckmann S A and Yakacki C M 2016 Copper-coated liquid-crystalline elastomer via bioinspired polydopamine adhesion and electroless deposition *Macromolecular rapid communications* **37** 1912–17
[30] He Q, Wang Z, Wang Y, Minori A, M T Tolley and Cai S 2019 Electrically controlled liquid crystal elastomer–based soft tubular actuator with multimodal actuation *Science Adv.* **5** eaax5746
[31] Shahinpoor M 2000 Electrically activated artificial muscles made with liquid crystal elastomers *Smart Structures and Materials 2000 Electroactive Polymer Actuators and Devices (EAPAD)* Int. Society for Optics and Photonics vol 3987 pp 187–93
[32] Finkelmann H and Shahinpoor M 2002 Electrically controllable liquid crystal elastomer-graphite composite artifical muscles *Smart Structures and Materials 2002 Electroactive Polymer Actuators and Devices (EAPAD)* Int. Society for Optics and Photonics vol 4695 pp 459–65
[33] Shenoy D K, ThomsenIII D L, Srinivasan A, Keller P and Ratna B R 2002 Carbon coated liquid crystal elastomer film for artificial muscle applications *Sensors Actuators* A **96** 184–8
[34] Chambers M, Zalar B, Remškar M, Žumer S and Finkelmann H 2006 Actuation of liquid crystal elastomers reprocessed with carbon nanoparticles *Appl. Phys. Lett.* **89** 243116
[35] Ford M J, Ambulo C P, Kent T A, Markvicka E J, Pan C, Malen J, Ware T H and Majidi C 2019 A multifunctional shape-morphing elastomer with liquid metal inclusions *Proc. of the National Academy of Sciences* p 201911021
[36] Fassler A and Majidi C 2013 3d structures of liquid-phase gain alloy embedded in pdms with freeze casting *Lab Chip* **13** 4442–50
[37] Majidi C 2014 Soft robotics: a perspective—current trends and prospects for the future *Soft Robot.* **1** 5–11
[38] Boley J W, White E L, Chiu G T-C and Kramer R K 2014 Direct writing of gallium-indium alloy for stretchable electronics *Adv. Funct. Mater.* **24** 3501–7
[39] Bilodeau R A, White E L and Kramer R K 2015 Monolithic fabrication of sensors and actuators in a soft robotic gripper, *2015 IEEE/RSJ Int. Conf. on Intelligent Robots and Systems (IROS)* pp 2324–9
[40] Khoshmanesh K, Tang S-Y, Zhu J Y, Schaefer S, Mitchell A, Kalantar-Zadeh K and Dickey M D 2017 Liquid metal enabled microfluidics *Lab Chip* **17** 974–93
[41] Yang J, Cheng W and Kalantar-Zadeh K 2019 Electronic skins based on liquid metals *Proc. of the IEEE* https://doi.org/10.1109/JPROC.2019.2908433
[42] Kim T, Kim D-m, Lee B J and Lee J 2019 Soft and deformable sensors based on liquid metals *Sensors* **19** 4250
[43] Wang X, Guo R and Liu J 2019 Liquid metal based soft robotics: materials, designs and applications *Adv. Mater. Technol.* **4** 1800549
[44] Black J R 1969 Electromigration—a brief survey and some recent results *IEEE Trans. Electron Devices* **16** 338–47
[45] Tu K, Yeh C, Liu C and Chen C 2000 Effect of current crowding on vacancy diffusion and void formation in electromigration *Appl. Phys. Lett.* **76** 988–90
[46] Michaud H O and Lacour S P 2019 Liquid electromigration in gallium-based biphasic thin films *APL Mater.* **7** 031504
[47] Ma R, Guo C, Zhou Y and Liu J 2014 Electromigration induced break-up phenomena in liquid metal printed thin films *J. Electron. Mater.* **43** 4255–61
[48] Yakacki C, Saed M, Nair D, Gong T, Reed S and Bowman C 2015 Tailorable and programmable liquid-crystalline elastomers using a two-stage thiol–acrylate reaction, *RSC Adv.* **5** 18997–9001
[49] Lu T, Markvicka E J, Jin Y and Majidi C 2017 Soft-matter printed circuit board with uv laser micropatterning *Acs Appl. Mater. Inter.* **9** 22055–62
[50] Jeong S, Hjort K and Wu Z 2014 Tape transfer printing of a liquid metal alloy for stretchable rf electronics *Sensors* **14** 16311–21
[51] Roberts P, Damian D D, Shan W, Lu T and Majidi C 2013 Soft-matter capacitive sensor for measuring shear and pressure deformation *2013 IEEE Int. Conf. on Robotics and Automation* pp 3529–34

[52] Plucinsky P P 2017 *The deformations of thin nematic elastomer sheets PhD thesis*, California Institute of Technology
[53] Saed M O, Torbati A H, Starr C A, Visvanathan R, Clark N A and Yakacki C M 2017 Thiol-acrylate main-chain liquid-crystalline elastomers with tunable thermomechanical properties and actuation strain *J. Polym. Sci.* B **55** 157–68
[54] Madden J D *et al* 2004 Artificial muscle technology: physical principles and naval prospects *IEEE J. Ocean. Eng.* **29** 706–28
[55] Lu H-F, Chen X-M, Lin B-P and Yang H 2019 Interpenetrating liquid-crystal polyurethane/polyacrylate elastomer with ultrastrong mechanical property *J. Am. Chem. Soc.* **141** 14364–9
[56] Petsch S, Rix R, Khatri B, Schuhladen S, Müller P, Zentel R and Zappe H 2014 Smart artificial muscle actuators: Liquid crystal elastomers with integrated temperature feedback *Sensors Act. A: Phys.* **231** 44–51
[57] Dutta I and Kumar P 2009 Electric current induced liquid metal ow: Application to coating of micropatterned structures *Appl. Phys. Lett.* **94** 184104